



HAL
open science

High temperature performance of recycled fine concrete

Nonna Algourdin, C. Bideux, Zyed Mesticou, Amir Si Larbi

► **To cite this version:**

Nonna Algourdin, C. Bideux, Zyed Mesticou, Amir Si Larbi. High temperature performance of recycled fine concrete. *Low-carbon Materials and Green Construction*, 2024, 2 (1), pp.19. 10.1007/s44242-024-00050-w . hal-04845293

HAL Id: hal-04845293

<https://ec-lyon.hal.science/hal-04845293v1>

Submitted on 18 Dec 2024

HAL is a multi-disciplinary open access archive for the deposit and dissemination of scientific research documents, whether they are published or not. The documents may come from teaching and research institutions in France or abroad, or from public or private research centers.

L'archive ouverte pluridisciplinaire **HAL**, est destinée au dépôt et à la diffusion de documents scientifiques de niveau recherche, publiés ou non, émanant des établissements d'enseignement et de recherche français ou étrangers, des laboratoires publics ou privés.



Distributed under a Creative Commons Attribution 4.0 International License

ORIGINAL ARTICLE

Open Access



High temperature performance of recycled fine concrete

N. Algourdin^{1*}, C. Bideux¹, Z. Mesticou¹ and A. Si Larbi¹

Abstract

The objective of this study is to explore the physical and mechanical behaviour of concretes comprising four different ratios of recycled fine (RF), namely (5%, 10%, 15% and 20%) along with that of a reference concrete (Cref-0%), under three different heating–cooling cycles (200 °C, 400 °C and 600 °C). The thermal properties of concrete during heating and cooling (20 °C – 600 °C – 20 °C) were also investigated. It was determined that the physical properties (mass loss and ethanol porosity) of recycled concrete (RC) with 5% of recycled fine (RC-5%) were similar to those of Cref-0%. At ambient temperatures, the higher the ratio of recycled fines, the lower the residual compressive strength and residual elastic modulus of the recycled concrete. After thermal loading at 600 °C, the residual mechanical properties of all types of concrete were equivalent, regardless of the content recycled fine.

Keywords High temperatures, Recycled concrete, Thermal properties, Residual mechanical properties

摘要

本研究的目的是探索四种不同再生细骨料 (RF) 取代率 5%、10%、15% 和 20% 的混凝土以及参照组混凝土 (Cref-0%) 在三种不同加热–冷却循环温度下 (200 °C、400 °C 和 600 °C) 的物理和力学性能。研究还分析了再生细骨料混凝土在加热和冷却 (20 °C–600 °C–20 °C) 过程中的热学性能。结果表明, 含 5% 再生细骨料 (RC-5%) 的再生混凝土 (RC) 的物理性能 (质量损失和孔隙率) 与参照组混凝土 (Cref-0%) 相近。在室温下, 再生细骨料掺量越高, 再生混凝土的残余抗压强度和残余弹性模量越低。在 600 °C 热载荷后, 所有种类的混凝土的残余力学性能均相当, 且与再生细骨料掺量无关。

关键词 高温, 再生混凝土, 热学性能, 残余力学性能

1 Introduction

In France, the construction sector is the largest consumer of natural resources and the largest producer of waste, generating more than 500 million tonnes of extracted aggregates and 300 million tonnes of waste annually [1]. The current issue is organising circular economies to reduce the impact of the construction sector on the environment. To achieve success, all participants in the

construction field must agree that there should be no normative, technical, legislative, or economic obstacles to favour the development of new construction sectors.

Portland cement contributes to over 80% of the carbon dioxide emissions in concrete production. A large portion of these emissions is caused by the decarbonation of limestone from the raw material. Reduced-carbon cements, such as alkali-activated cements [14] and calcium aluminate, have been used to reduce the clinker content [22]. The problems with these new cements are their high price and long-term implementability [19].

Recent research has indicated the possibility of reusing recycled fines (RF) to replace cement in concrete [6–8, 12]. The results of these studies are promising. Algourdin

*Correspondence:

N. Algourdin
nonna.algourdin@enise.fr

¹ UMR 5513, ENISE, Université de Lyon, Ecole Centrale de Lyon, CNRS, ENTPE, LTDS, 42023 Saint-Etienne, France

et al. [11] noted that RF contains many hydrates such as calcium silicate hydrate (C-S-H), ettringite, and portlandite, which could potentially be rehydrated. Moreover, Shui et al. [33] concluded that RF exhibits a nonzero cumulative heat release and ionic activity during the rehydration process. Florea et al. [16] concluded that 20% of cement could be replaced by recycled fines without significant loss of strength.

Research on the influence of high temperatures on concrete, including RF, is rare, and only limited data are available. Concerning the thermal properties, some authors [9, 32] have indicated that the thermal conductivity of concrete with RF decreases significantly under elevated temperatures owing to the higher porosity of RF. It is evident that RF influences the free water content and porosity of recycled concrete (RC). These properties influence the thermal and mechanical behaviours of RC at ambient and high temperatures. Several studies were carried out on the residual mechanical properties of recycled aggregate concrete at elevated temperatures [21, 25, 37]. However, to the best of our knowledge, there are no studies on the mechanical “hot” or residual properties of recycled fine concretes (RFC). This lack of information necessitates an improvement in the fundamental understanding of the impact of elevated temperatures on the RF concrete.

Several studies have observed the following stages in the degradation of cement matrix during the rise of the temperature [5, 10, 11, 30]: From ambient temperature to 130 °C the loss of capillary free adsorbed water is observed, from 130 °C to 170 °C the double endothermic reaction of gypsum decomposition; from 150 °C to 300 °C partial loss of bound water from the hydrates and C-S-H gel; from 450 °C to 550 °C portlandite decomposition, and from 600 °C to 750 °C C-S-H decomposition, β -C₂S formation, and calcium carbonate decomposition.

To fill in the gaps in literature, in this study the residual physical and mechanical properties of RFC with substitution rates of 5%, 10%, 15% and 20% of RF were examined. The evolution of heat transfer properties in “hot” conditions allows a better understanding of the behaviour of RFC during the heating and cooling processes. Furthermore, the characterisation of the residual resistance is very important for enhancing the fire performance of buildings, including that of RF.

2 Experimental methodology

2.1 Materials

Portland cement, CEM I 52.5 R, with a density of 3.1 kg.L⁻¹, $w(\text{SO}_3) \leq 4.5\%$, $w(\text{Cl}^-) \leq 0.10\%$ and a start of hardening at 20 °C measured on pure paste ≥ 40 min was used in this study. Recycled sand (RS) (0/5 mm) from a recycling platform was sieved to obtain 0/80 μm fraction. This fraction was used to substitute the 5%, 10%, 15%, and 20% of mass of Portland cement in recycled concrete. The dispersion of the recycled fine was made with OCCHIO500 nano XY image analyser and showed in Fig. 1.

Siliceous gravel and siliceous-calcareous sand composed of flints (70% – 75%), calcium carbonate (20% – 25%), and feldspar (5%) with fractions of 25/125 mm and 0/5 mm, respectively. The grain size distribution is showed in Fig. 2.

2.2 Mixture proportions designs

Five concrete mixtures were studied: Cref-0% (concrete without recycled fines), RC-5%, RC-10%, RC-15%, and RC-20%, that is, concrete with 5%, 10%, 15%, and 20% of RF, respectively. The water/binder (W/B) ratio for all the concrete mixtures was constant at 0.5. The slump of the concrete ranged from 10 mm –130 mm. The concrete mix proportions are presented in Table 1.

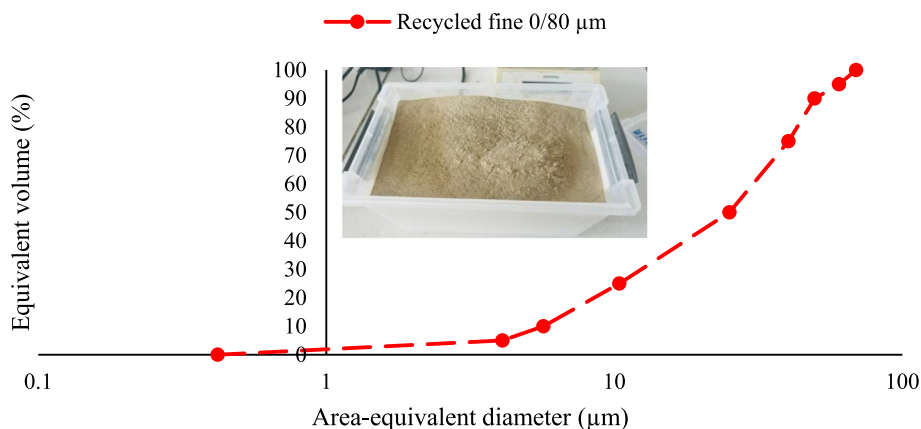


Fig. 1 Grain size distribution of the used recycled fine

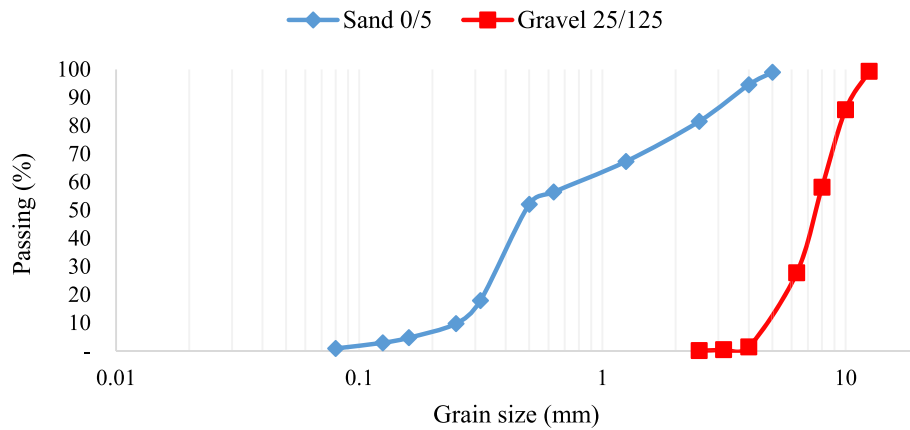


Fig. 2 Grain size distribution of the used siliceous gravel and siliceous-calcareous sand

Table 1 Mix proportions of concretes (kg/m³)

| Concrete | Physical quantities | | | | |
|----------|---------------------|---------------|-----------------|----------|-----------------|
| | Cement | Recycled fine | Gravel 2.5/12.5 | Sand 0/5 | Effective water |
| Cref-0% | 400 | 0 | 1 047 | 705 | 200 |
| RC-5% | 380 | 20 | 1 057 | 711 | 200 |
| RC-10% | 360 | 40 | 1 067 | 718 | 200 |
| RC-15% | 340 | 60 | 1 077 | 725 | 200 |
| RC-20% | 320 | 80 | 1 087 | 732 | 200 |

2.3 Curing conditions

Cylindrical concrete specimens with dimensions of 150 mm×300 mm and 110 mm×220 mm were cast. The RILEM (200-HTC) procedure [29] was applied to all the mixtures. The specimens were retained in their moulds for seven days to prevent any evaporation of moisture and, then placed in sealed plastic bags at 20±2 °C with a damp cloth to maintain a humid atmosphere for at least during 90 d, until the heating.

2.4 Heating tests

The heating tests were performed in an electric furnace (Fig. 3) having dimensions 1 950 mm×2 000 mm×1 550 mm (L×h×d).

Ten type-K thermocouples were integrated using a Programmable Logic Controller (PLC) to program the temperature, for temperature monitoring, control, and regulation in real time and for security management. The thermocouples were positioned to monitor the temperature in the furnace, on the surface of the specimen, and at the centre of the concrete cylinder. Three specimens per mix were prepared with type K thermocouples at the centre of the concrete (embedded thermocouple at mid-height and mid-diameter of the concrete cylinder).



Fig. 3 Exterior of electric furnace

As the incorporation of a thermocouple could affect the temperature distribution and strength of the specimens, the specimens with the thermocouples at the centre were not used for subsequent tests. Data was acquired every 30 s. The surface temperature of the specimen controlled the increase in temperature in the furnace.

The thermal properties were measured under “hot” conditions, from ambient temperature up to 600 °C and

from 600 °C down to ambient temperature (20 °C – 600 °C – 20 °C). The measurements were taken every 50 °C with the heating rate at 0.5 °C/min. No cooling phase was applied. Each point on the graph represents the average of five values obtained for three concrete samples. There was a delay of 1 h between measurements to avoid any possible disturbances from the previous measurement.

To determine the residual properties, three heating–cooling cycles were applied, one each for the phase of rise in temperature at the rate of 0.5 °C/min, a phase of temperature dwell (2 h), and a cooling phase. The 150 mm × 300 mm and 110 mm × 220 mm concrete cylinders were subjected to temperatures from the room temperature to 200 °C, 400 °C and 600 °C (Fig. 4).

2.5 Characterisation tests

Different tests were performed to characterise the recycled concrete, as described below. The evolution of the concrete microstructure was studied using the total porosity and X-ray tomography. Water and heat transfers were investigated based on mass loss and thermal properties. The compressive strength (f_c) and the elastic static (E_{stat}) and dynamic (E_{dyn}) moduli were determined to estimate the influence of the recycled fines on the residual mechanical properties.

All conditions for all the tests, including the specimen geometry and heating cycles, are listed in Table 2. The number of specimens for each test corresponds to the required number by European standards.

2.5.1 Mass loss

The mass loss of the specimen was obtained for three cylindrical specimens with dimensions of 150 mm × 350 mm for each cycle. The specimens were weighed before

and after each heating–cooling cycle to calculate the quantity of concrete mass loss during heating.

2.5.2 Ethanol accessible porosity (P_{tot})

Four samples with an average mass of 400 g for each concrete and each heating–cooling cycle were used. Measurements were performed using ethanol to prevent rehydration of portlandite and C-S-H gel. The specimens were oven-dried at 80 °C or heated to 200 °C, 400 °C or 600 °C until a constant mass was obtained. The specimens were placed in a vacuum cell for air extraction and ethanol filling [2]. After 24 h of immersion, the samples were weighed immediately after the pump was disconnected.

2.5.3 X-ray tomography observation

The recycled concrete samples were cut into cubes (30 mm × 30 mm × 30 mm) and analysed using SkyScan tomography. Scanning was performed using a slice-by-slice technique with an exposure time of 400 ms, rotation angle of 0.5°, and accelerating voltage of 85 kV.

2.5.4 Thermal properties (λ, a)

A Hot Disk TPS 1500 device, based on the principle of the transient plane source (TPS) method, was used. This method involves applying a thermal disturbance to a sample at isothermal equilibrium and measuring the temperature over a period of time. The samples were placed in an oven at 80 °C until the constant mass (about 3 weeks). Before testing, the specimens are removed from the oven for cooling and placed in sealed bags to preserve their water content. To ensure that the samples do not present a thermal gradient, after reaching the required temperature, the specimens remain on same temperature plateau during 30 min before the measurement.

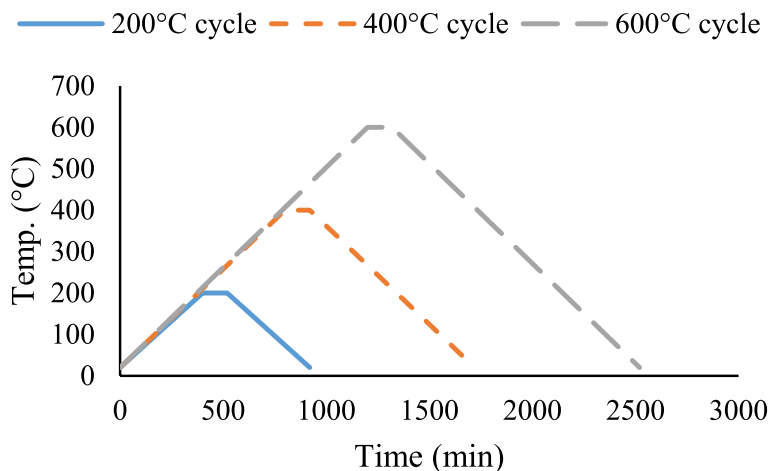

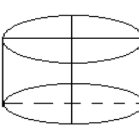


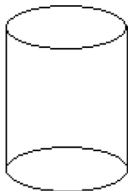
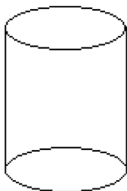
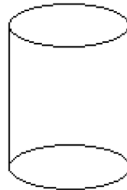


Fig. 4 Thermal profiles of the heating–cooling cycles

Table 2. Summary of tests during or after heating including specimen geometry and heating steps

| Tests | Type and number of specimens, | Heating conditions |
|---|--|---|
| | mm | |
| Mass loss (three specimens per mix) |  150 × 35 | 80 °C, 200 °C, 400 °C, 600 °C |
| Porosity (four specimens per mix) |  ¼ of sample; 150 (∅) × 50 | 80 °C, 200 °C, 400 °C, 600 °C |
| X-ray tomography (four specimens per mix) |  (30 × 30 × 30) | 80 °C, 600 °C |
| Thermal properties: conductivity and diffusivity (three specimens per mix × two slices) |  110 (∅) × 40 | From 20 °C to 500 °C and from 500 °C to 20 °C |
| Thermal response (2–3 specimens per mix) |  110 (∅) × 220 | 600 °C Heating rate: 0.5 °C/min |
| Compressive strength (f_c) (four specimens per mix) |  110 (∅) × 220 | 20 °C, 200 °C, 400 °C, 600 °C |
| Dynamic (E_{dyn}) and static (E_{stat}) elastic moduli (four specimens per mix) |  110 (∅) × 220 | 20 °C, 200 °C, 400 °C, 600 °C |

The device is composed of a furnace of capacity 5 L that can attain a temperature of 1 200 °C, a computer, and an automatic data acquisition unit with a Hot Disk probe connection (Fig. 5).

A Kapton probe having a radius of 9.868 mm was used for the tests at ambient temperature, and a mica probe having a radius of 14.610 mm was used for the tests at higher temperatures.

2.5.5 Compressive strength

For each mix and for each heating–cooling cycle, four 110 mm (\varnothing) \times 220 mm specimens were tested with uniaxial compressive loading with an imposed stress rate of 0.5 MPa.s⁻¹ according to European standard EN 12390-3[4].

2.5.6 Determination of elastic static modulus

For each mix and for each heating–cooling cycle, tests were carried out on the four 110 mm (\varnothing) \times 220 mm cylindrical specimens. During the compression test, each specimen was connected to an extensometer frame and subjected to three loading–unloading cycles with a 20 s dwell. The loading rate was 0.5 MPa.s⁻¹ according to European standard EN 12390-13[3].

2.5.7 Determination of elastic dynamic modulus

To determine the dynamic Young's modulus, a Pundit Lab device was used to measure ultrasonic wave propagation [26]. The device emitted an electric signal through the specimen, which was then converted into waves using a piezoelectric transducer. Petroleum jelly was used to ensure perfect contact between the face of each transducer and concrete sample. The wave propagated in the specimen from one transducer to the other, and was then reflected back to the first transducer. The apparatus measured the time t between two successive echoes, based on which the longitudinal ultrasonic wave speed could be calculated as $V=L/t$, where V is the ultrasonic

wave speed [in m/s], L is the length of the cross-piece material [in m], and t is the time required for wave propagation along length L [in μ s].

The dynamic Young's modulus was calculated using the following relationship: E [in GPa] = $\rho \times (V^2 (1 + U) (1 - 2U)) / (1 - U)$, where V is the ultrasonic wave speed [in m/s], ρ is the concrete density [in kg/m³] measured after each heating cycle, and U is Poisson's ratio (considered as 0.2 for concrete).

3 Results and discussion

No spalling phenomenon was observed during the heating–cooling phases.

Table 3 presents all the results of the experiment for Cref-0%, RC-5%, RC-10%, RC-15%, and RC-20% concretes.

3.1 Physical properties

Table 3 summarises the physical properties (mass loss and ethanol porosity) of Cref-0%, RC-5%, RC-10%, RC-15%, and RC-20% concrete. For the residual porosity, the standard deviation (SD) was low and almost unnoticeable on the graph.

3.1.1 Mass loss

Figure 6 shows the evolution of Cref-0%, RC-5%, RC-10%, RC-15%, and RC-20% concrete mass losses as a function of temperature. For all specimens, the mass loss increased with temperature. Between 20 °C and 200 °C, the mass loss is essentially due to the loss of free water, the water contained in the pores, adsorbed water on the surface of the solid elements, and bound water. The maximum difference in mass loss in this temperature region (200 °C) was 0.2%. Between 200 °C and 400 °C the C-S-H dehydration leads to relatively low mass loss with an average value of 2%. Between 400 °C and 600 °C the Portlandite dehydroxylation increases the mass loss by 1.8% on average.

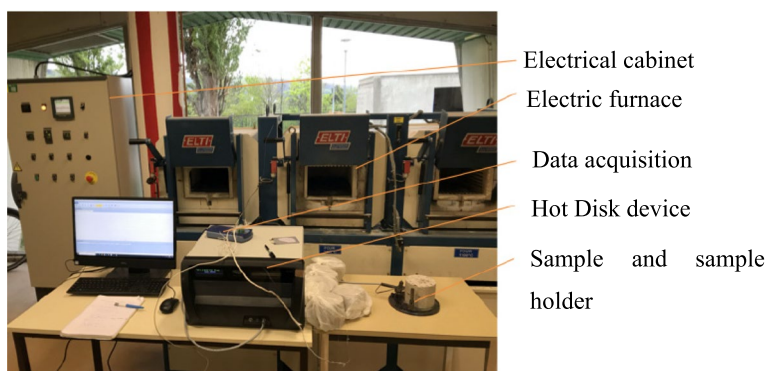


Fig. 5 Setup for measurement of thermal properties/parameters

Table 3 Physical, thermal and mechanical properties of concretes

| Concretes | Drying/ Heating rate °C | Mass loss | | Ethanol porosity (P_{tot}) | | Thermal conductivity | | Thermal diffusivity | | Compressive strength | | Elastic static modulus | | Elastic dynamic modulus | |
|-----------|----------------------------------|-----------|------|--------------------------------------|------|-------------------------|------|------------------------|------|-------------------------|------|---------------------------|------|----------------------------|------|
| | | % | SD | % | SD | W/(m·K) | SD | mm ² /s | SD | MPa | SD | GPa | SD | GPa | SD |
| Cref-0% | 20 | | | | | | | | | 64.3 | 1.00 | 36.6 | 0.37 | 45.2 | 0.19 |
| | 80 | | | 9.7 | 0.08 | 2.1 | 0.02 | 1.6 | 0.01 | | | | | | |
| | 200 | 3.6 | 0.18 | 10.4 | 0.17 | 1.9 | 0.07 | 0.9 | 0.03 | 62.0 | 1.90 | 29.7 | 0.54 | 37.9 | 0.27 |
| | 400 | 5.5 | 0.03 | 12.4 | 0.21 | | | | | 45.1 | 1.77 | 23.5 | 3.85 | 23.2 | 1.92 |
| | 500 | | | | | 1.7 | 0.08 | 0.6 | 0.04 | | | | | | |
| | 600 | 6.9 | 0.09 | 18.0 | 0.21 | | | | | 18.0 | 1.62 | 5.1 | 2.33 | 4.3 | 1.17 |
| RC-5% | 20 | | | | | | | | | 60.7 | 2.11 | 36.0 | 0.03 | 44.6 | 0.01 |
| | 80 | | | 11.5 | 0.11 | 2.0 | 0.02 | 1.1 | 0.06 | | | | | | |
| | 200 | 3.7 | 0.29 | 11.6 | 0.20 | 1.9 | 0.10 | 0.7 | 0.04 | 57.0 | 3.00 | 33.0 | 3.79 | 38.4 | 1.89 |
| | 400 | 6.2 | 0.21 | 13.4 | 0.30 | | | | | 35.2 | 1.89 | 11.8 | 0.96 | 19.4 | 0.48 |
| | 500 | | | | | 1.5 | 0.03 | 0.4 | 0.04 | | | | | | |
| | 600 | 7.6 | 0.04 | 19.0 | 0.19 | | | | | 13.0 | 1.68 | 5.5 | 1.97 | 3.1 | 0.99 |
| RC-10% | 20 | | | | | | | | | 57.5 | 2.10 | 32.9 | 0.02 | 40.6 | 0.00 |
| | 80 | | | 13.1 | 0.09 | 2.0 | 0.10 | 1.3 | 0.05 | | | | | | |
| | 200 | 3.6 | 0.35 | 14.4 | 0.25 | 1.7 | 0.08 | 0.7 | 0.04 | 54.0 | 2.08 | 28.8 | 1.05 | 34.5 | 0.53 |
| | 400 | 5.7 | 0.69 | 15.6 | 0.17 | | | | | 29.0 | 1.94 | 12.3 | 0.36 | 19.8 | 0.18 |
| | 500 | | | | | 1.5 | 0.10 | 0.4 | 0.05 | | | | | | |
| | 600 | 7.7 | 0.10 | 20.8 | 0.12 | | | | | 14.0 | 1.69 | 4.2 | 0.38 | 4.1 | 0.18 |
| RC-15% | 20 | | | | | | | | | 51.3 | 2.13 | 29.3 | 0.12 | 41.1 | 0.06 |
| | 80 | | | 12.5 | 0.18 | 2.0 | 0.12 | 1.3 | 0.05 | | | | | | |
| | 200 | 3.8 | 0.42 | 14.0 | 0.23 | 1.9 | 0.09 | 0.7 | 0.03 | 49.0 | 1.93 | 29.0 | 1.58 | 36.4 | 0.79 |
| | 400 | 5.9 | 0.10 | 14.7 | 0.38 | | | | | 32.0 | 1.79 | 12.2 | 1.55 | 18.5 | 0.78 |
| | 500 | | | | | 1.5 | 0.09 | 0.2 | 0.06 | | | | | | |
| | 600 | 7.9 | 0.77 | 19.0 | 0.04 | | | | | 16.0 | 3.00 | 4.4 | 1.60 | 3.6 | 0.80 |
| RC-20% | 20 | | | | | | | | | 49.3 | 2.10 | 28.9 | 0.57 | 40.3 | 0.28 |
| | 80 | | | 12.5 | 0.18 | 2.0 | 0.02 | 1.2 | 0.06 | | | | | | |
| | 200 | 3.8 | 0.02 | 13.0 | 0.06 | 1.9 | 0.10 | 0.7 | 0.04 | 46.0 | 2.00 | 27.5 | 0.69 | 33.7 | 0.34 |
| | 400 | 5.5 | 0.09 | 14.9 | 0.19 | | | | | 30.0 | 1.88 | 12.2 | 0.04 | 19.6 | 0.02 |
| | 500 | | | | | 1.5 | 0.03 | 0.4 | 0.04 | | | | | | |
| | 600 | 7.6 | 0.17 | 20.3 | 0.32 | | | | | 10.0 | 1.65 | 4.2 | 1.39 | 4.7 | 0.69 |

Cref-0% concrete showed lower mass loss than recycled concrete. This was due to the higher rate of water loss from the recycled concrete. Fig. 8 corroborates these results; the porosity of Cref-0% concrete showed lower evolution compared to the other recycled concrete mixtures. Furthermore, the higher water absorption of the recycled fines results in a higher water release at elevated temperatures [31].

Figure 7 shows the mass loss for different RF content (0 – 20%) for three temperatures (200 °C, 400 °C, and 600 °C). For 200 °C, the variation in mass loss for all formulations is not significant with the maximum being 0.2%. It becomes significant for 400 °C and 600 °C, where the variation is 0.7% and 1.1%, respectively [20, 36]. In this range

of temperatures, with RF varying from 0 to 5%, the mass loss increased slightly and did not vary much thereafter.

3.1.2 Ethanol accessible porosity

Figure 8 shows the evolution of the absolute porosity of the reference and recycled concretes as a function of temperature. Porosity increases slightly between 80 °C and 400 °C; however, beyond 400 °C the slope of the porosity curve is significant. In the case of heat treatment of the concrete, porosity evolution is essentially linked to microstructural degradation or the appearance of cracks. Other phenomena such as pore coalescence do not play a predominant role in pore transformation. As seen on X-ray tomography, cracking becomes visible at 600 °C. In

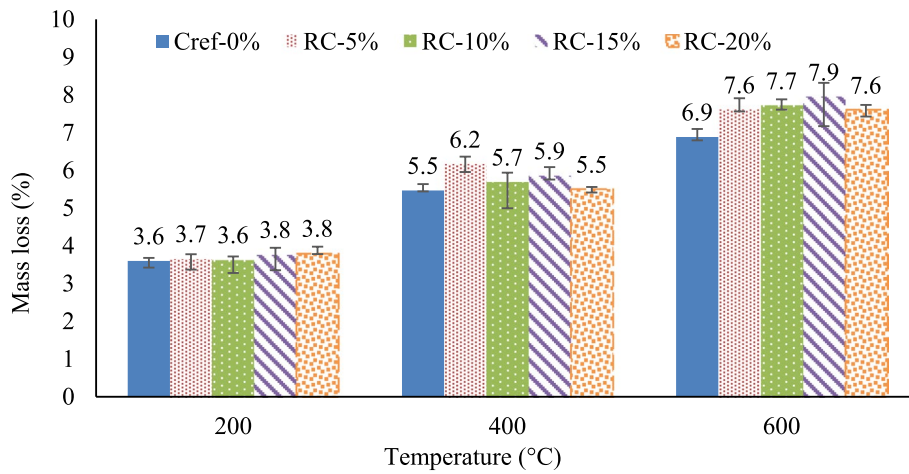


Fig. 6 Mass loss evolution of the concrete mixes as a function of temperature

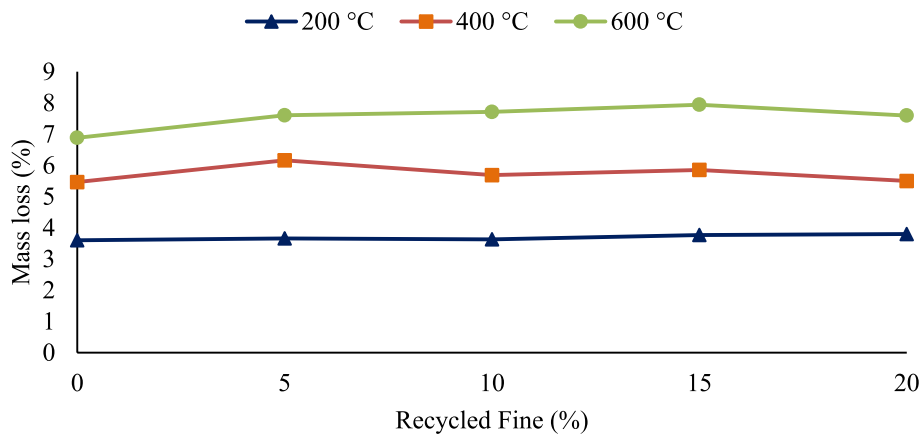


Fig. 7 Effect of RF content on the mass loss

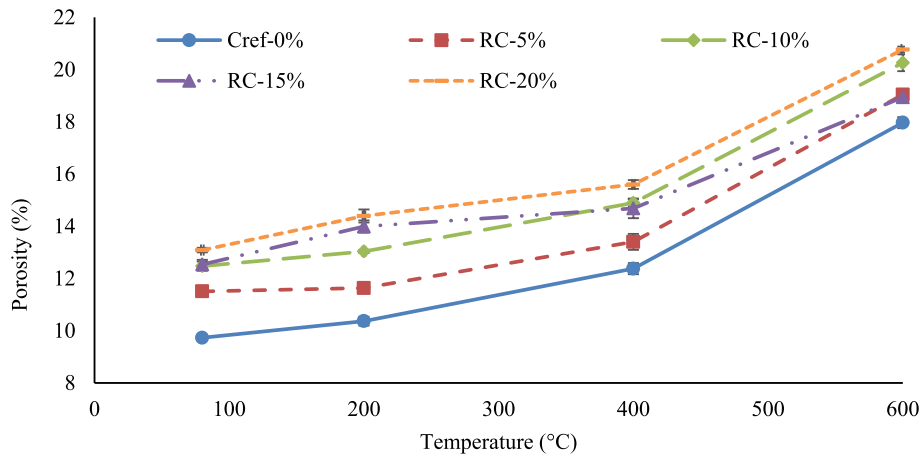


Fig. 8 Evolution of the porosity of residual ethanol as a function of exposure temperature

addition, the increase in porosity between 80 °C and 200 °C is associated with the most intense mass loss (Fig. 6), and is the result of C-S-H dehydration. This in most cases lasts up to 300 °C.

Although the porosity values for the different concrete formulations are comparable, recycled concrete exhibits a higher porosity during the entire heating phase. Moreover, the absolute porosities of RC-10% and RC-15% are very close. The addition of recycled fines increases the porosity of recycled concrete. This is consistent with the results of previous studies [8, 11]: poor workability leads to more pores in the recycled concrete. This is due to the larger surface area of the recycled particles and the porous morphology of the dehydrated compounds. In addition, higher the RF rate, higher the porosity of recycled concrete.

3.1.3 X-ray tomography

Three-dimensional (3D) X-ray microtomography slices of the Cref-0% and RC-20% concrete are shown in Fig. 9 and Fig. 10. The RC-20% concrete was the most damaged

by the heating, therefore was chosen for X-ray tomography observation. A visual inspection of the images indicates an increase in the pore network at 600 °C for the two concretes (Cref-0% and RC-20%). This was consistent with the ethanol porosity and residual mechanical property results (see below). Additionally, as suggested by Kim et al. [23] the variation in the volume of the pores during heating can be a quantitative indicator for analysing the damage caused to concrete by high temperatures.

From the 3D slices, it can also be observed that some cracks appeared on RC-20% concrete after heating to 600 °C. In contrast, less cracks were observed on the four specimens of Cref-0% concrete after treatment at 600 °C. Cracks were mostly formed in the paste, and no cracks were observed at the paste/aggregate interface.

3.1.4 Thermal properties

Table 3 presents the thermal properties (thermal conductivity and thermal diffusivity) of Cref-0%, RC-5%, RC-10%, RC-15%, and RC-20% concretes. Thermal modelling of concrete should not consider only single values

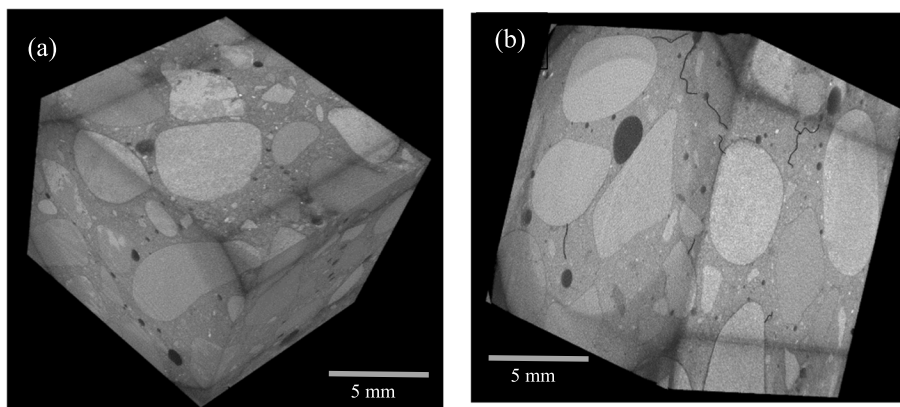


Fig. 9 3D X-ray slices of Cref-0% concrete at ambient temperature (a) and after heating to 600 °C (b)

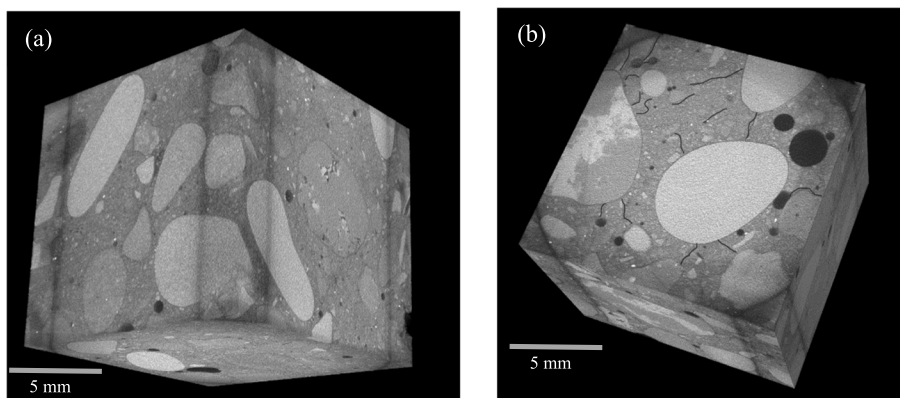


Fig. 10 3D X-ray slices of RC-20% concrete (a) at ambient temperature and (b) after heating to 600 °C

of conductivity and diffusivity at each temperature level, but should take into account the history of the thermal loading.

3.1.5 Thermal conductivity

Fig. 11 presents the thermal conductivity evolution of Cref-0%, RC-5%, RC-10%, RC-15% and RC-20% concretes during heating up to 500 °C and cooling up to 20 °C. The conductivities of all concretes decreased with increasing temperature. When the air conductivity is less (0.024 W/(m·K)) than that of concrete, it is evident that the conductivity decreases as the porosity increases. Another explanation for the decrease in conductivity concerns the increase in the vibrational energy of the phonons, as described by Algourdin et al. [9]. In fact, by heating the material, the number of phonons increases, increasing the number of collisions between them, thereby increasing the resistance vis-à-vis the heat flow.

The recycled concrete exhibited lower thermal conductivity than the Cref-0%. This was consistent with their higher total porosity values (see Sect. 3.1.2) [17]. Hysteresis was observed between heating and cooling phases, which can be explained by the majority of reactions that are irreversible, as departure of physically and chemically bound water or microcracks appearance, beyond 300 °C (see Sect. 3.1.3). Nevertheless, the aggregate expansion during heating is reversible and can partly explain the conductivity gain of RC-5% between 300 °C and 20 °C and of Cref-0%, RC-10% and RC-20% between 300 °C and 200 °C, during cooling.

The average loss of thermal conductivity from 20 °C to 500 °C for Cref-0% concrete is 0.4 W/(m·K) (~20%), and of recycled concretes is 0.5 W/(m·K) (~25%). These values are higher than those reported in the literature for concrete with recycled gravel and/or sand [9, 24].

Recycled fines (up to 20% in volume) do not have the same kind of determining influence on concrete as recycled gravel and sand.

3.1.6 Thermal diffusivity

The trends in the evolution of the thermal diffusivity are presented in Fig. 12. At ambient temperature, the Cref-0% concrete shows a higher value of thermal diffusivity (1.61 mm²/s) and the diffusivity of recycled concretes varies from 1.36 mm²/s to 0.84 mm²/s. These values are similar to those reported in the literature [13].

The thermal diffusivity decreased with temperature. This is consistent with the results of the total porosity, that is, higher porosity and lower diffusivity. For the recycled concrete, the difference in thermal diffusivity decreases with heating. The “hot” values of the thermal diffusivity (500 °C), represent approximately 32% of the diffusivity at room temperature: $a_{\text{Cref-0\%, 500 °C}} = 37.3\%$, $a_{\text{RC-5\%, 500 °C}} = 31.9\%$, $a_{\text{RC-10\%, 500 °C}} = 33.2\%$, $a_{\text{RC-15\%, 500 °C}} = 18.4\%$, $a_{\text{RC-20\%, 500 °C}} = 36.9\%$. Comparing these values with those of the thermal conductivity, it appears that the relative loss of the thermal diffusivity is greater than that of the thermal conductivity. During cooling, the diffusivity increases to regain 80%–90% of the initial value [27]. In the case of RC-5% and RC-15%, the diffusivities during cooling were slightly higher than those during heating. The increase in values fall within the standard deviation.

3.1.7 Thermal response

The temperature difference between the surface (T_{surf}) and the centre (T_{center}) of the specimens for the Cref-0%, RC-5%, RC-10%, RC-15% and RC-20% concretes during the heating–cooling cycle up to 600 °C is shown in Fig. 13. One endothermic peak and a slight increase are observed in the temperature difference curve. The

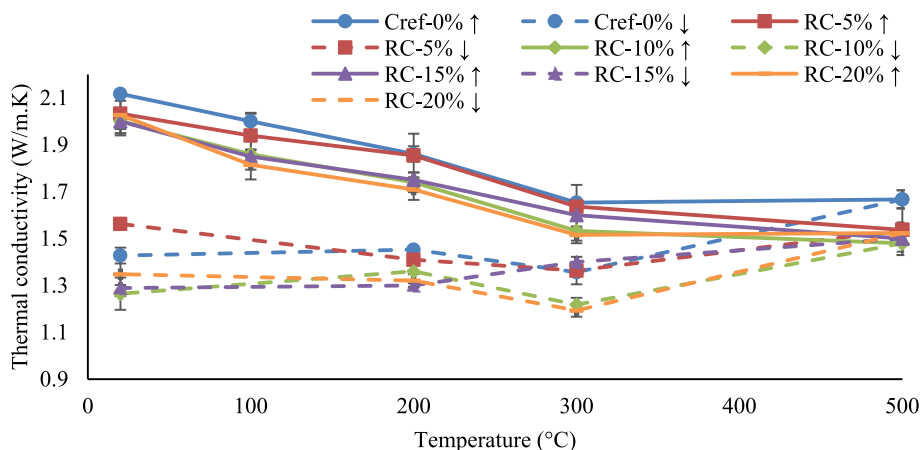


Fig. 11 Thermal conductivity evolution of Cref-0%, RC-5%, RC-10%, RC-15%, RC-20% concretes during heating (↑) and cooling (↓) phases

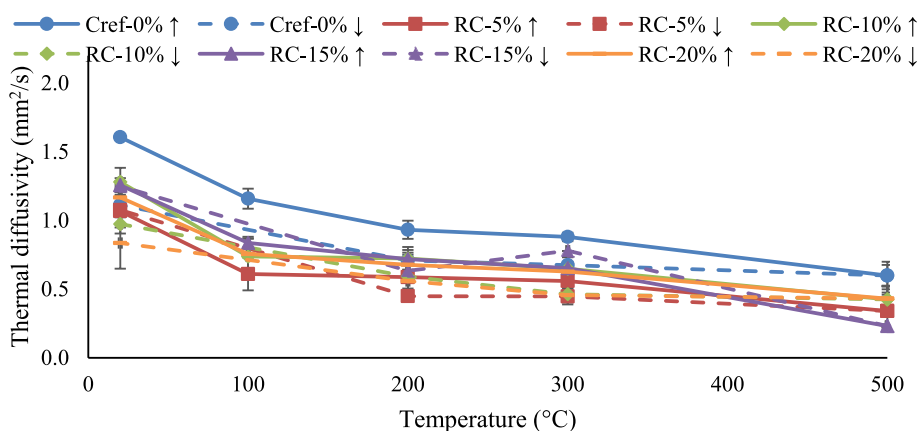


Fig. 12 Thermal diffusivity evolution of Cref-0%, RC-5%, RC-10%, RC-15%, RC-20% concretes with temperature during heating (↑) and cooling (↓) phases

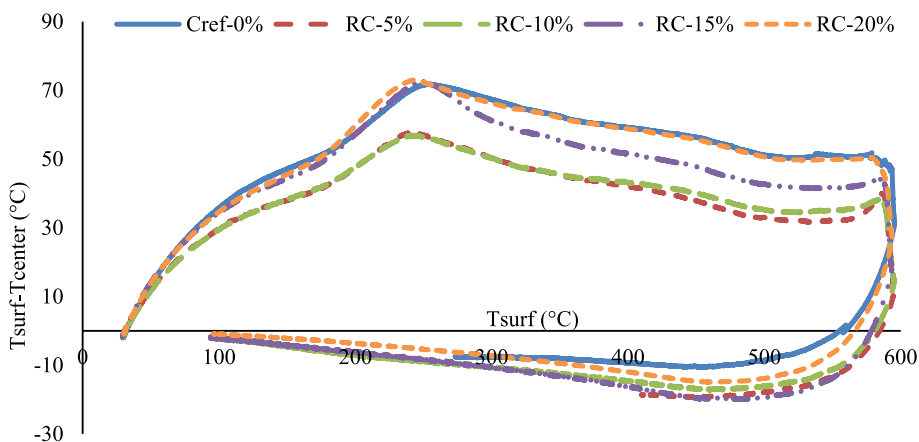


Fig. 13 Evolution of the temperature difference between the surface and the centre of the 150 mm × 300 mm concrete cylinders as a function of the surface temperature during heating-cooling cycles

endothermic peak appears between 200 °C and 300 °C and can be attributed to the consumption of latent heat due to C-S-H dehydration and water evaporation. Therefore, it is strongly linked to the quantity of water present in the material. The Cref-0%, RC-10% and RC-20% concretes produce higher peaks among the tested formulations with a ΔT of 15 °C, indicating higher presence of water. This result is consistent with the mass-loss values.

The beginning of the second rise, the highest being for RC-5% and RC-10% concretes, occurs around 600 °C (T_{surf}) and is related to the dehydroxylation of Portlandite. During cooling the temperature at the centre is 10 °C – 20 °C higher than that at the surface, which can cause additional cracking.

3.2 Residual mechanical properties

Table 3 summarises the results for the residual compressive strength (f_c), elastic static modulus (E_{stat}), and elastic

dynamic modulus (E_{dyn}) before and after each heating-cooling cycle.

3.2.1 Residual compressive strength

The absolute and relative compressive strengths are shown in Fig. 14 (a) and (b), respectively. By replacing cement with recycled fines, the compressive strength decreases with increasing replacement ratio. A 5% replacement of cement with RF reduces the 90 d compressive strength by only 5.7%, whereas 20% replacement reduces it by 23.3%. This decrease can be attributed to the high water absorption. This explanation is consistent with that offered in literature [15, 34].

For all concretes, the compressive strength decreases slightly until 200 °C and then the decrease is more significant between 200 °C and 600 °C. At the start of heating cycle, the drying process induces the following reaction: $Si-OH-HO-Si \rightarrow Si-O-Si + H_2O \uparrow$ and causes an

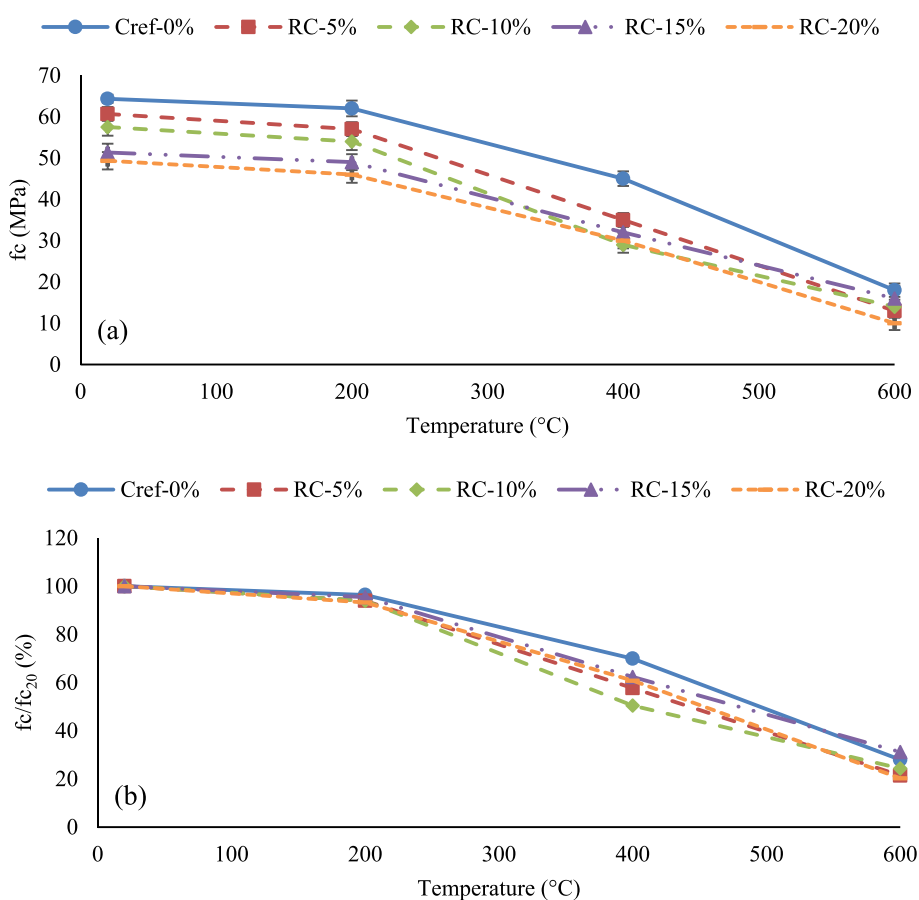


Fig. 14 Absolute (a) and relative (b) residual compressive strengths of Cref-0%, RC-5%, RC-10%, RC-15%, RC-20% concretes as a function of temperature

increase in the surface forces between the C-S-H gel particles which results in an increase in the resistance of the cement paste (recycled and reference). When the threshold of 300 °C is exceeded, the concrete no longer contains water and the strength decreases faster under the effect of increased temperature [18, 28].

The total porosity evolution was in good agreement with the compressive strength, and the two are inversely related. The total drop in the relative compressive strength of the recycled concretes is approximately 75%: Δf_c RC-5% = 78.6%, Δf_c RC-10% = 75.7%, Δf_c RC-15% = 68.8% and Δf_c RC-20% = 79.7% (Fig. 14 (b)). The total decrease in relative compressive strength of reference concrete is of 72.0%. This confirms that the recycled fine has a non-negligible degree of binding.

3.2.2 Elastic modulus

Figure 15 presents the absolute (a) and relative (b) residual elastic static moduli of the tested concretes as functions of temperature. At ambient temperatures, the elastic static modulus is strongly dependent on the

density of concrete. It varies from 29.0 GPa (more porous concrete) and 36.6 GPa (less porous concrete). Like the residual compressive strength, the elastic modulus decreases slightly between 20 °C and 200 °C. After 200 °C the decreases is higher and almost linear. Between 400 °C and 600 °C, all the recycled concretes showed practically the same drop of approximately 7 GPa. At 600 °C, the Cref-0% falls to the values for recycled concretes (E_{stat} Cref-0% = 5.1 GPa, E_{stat} RC-5% = 5.5 GPa, E_{stat} RC-10% = 4.2 GPa, E_{stat} RC-15% = 4.4 GPa, E_{stat} RC-20% = 4.3 GPa).

The residual elastic static modulus curves for the recycled concretes clearly show two drop modes, with a slow decrease in E_{stat} properties up to 200 °C and much faster decrease beyond 200 °C. The residual compressive strength exhibited a more linear loss in the performance of recycled concrete. These results are consistent with those reported previously [35, 38].

Figure 16 (a) and (b) show the absolute and relative residual elastic dynamic moduli, respectively, of the tested concretes as functions of temperature. The Cref-0% concrete shows higher values of the elastic dynamic

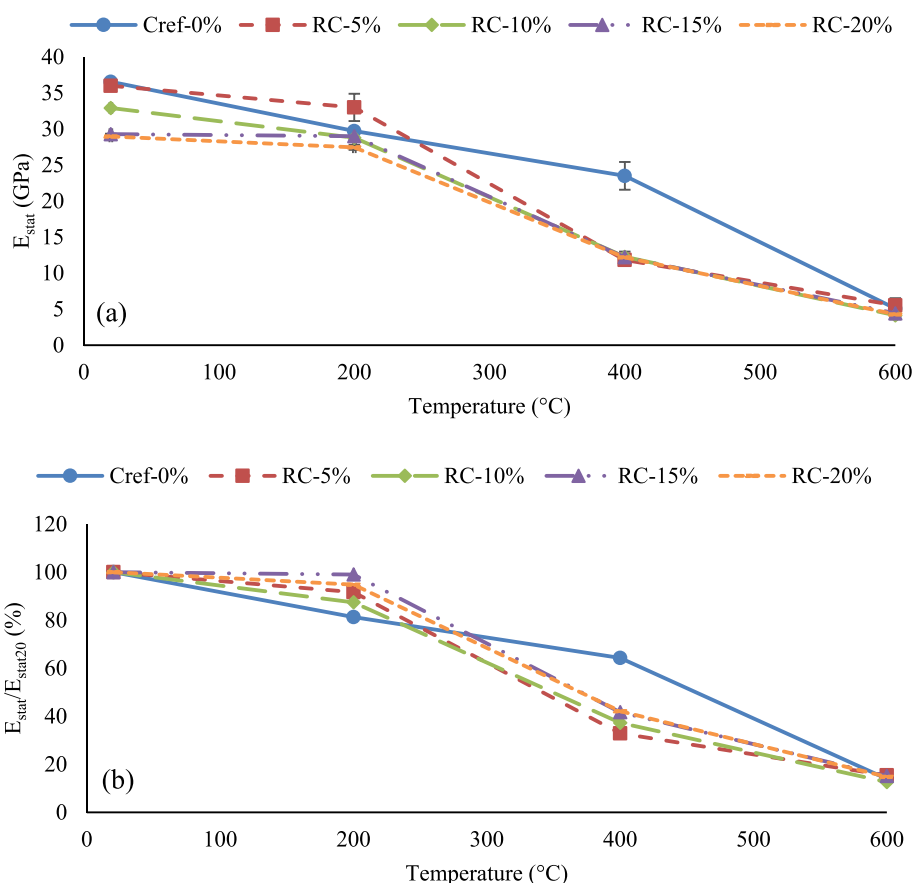


Fig. 15 Absolute (a) and relative (b) residual elastic static moduli of Cref-0%, RC-5%, RC-10%, RC-15%, RC-20% concretes as a function of temperature

modulus except at 200 °C. The same trend was observed for the static elastic modulus (Fig. 15). For the recycled concrete, the elastic dynamic modulus values were very close to the maximum delta of 4.7 GPa between RC-5% and RC-20% concretes after 200 °C. The elastic dynamic modulus of RC-5% concrete follows the same evolution as the Cref-0% concrete up to 200 °C, and it then drops to the values of other recycled concretes. After 600 °C, the E_{dyn} of all tested concretes varies between 3.1 GPa to 4.7 GPa.

The values of the elastic dynamic modulus were higher than those of the elastic static modulus, with an average difference of 10 GPa. Studies have shown that this difference is mostly due to two factors: the discrepancy in stress level during the tests and the intrinsic heterogeneity of the material, which causes an unequal response under cyclic or vibratory loading conditions. Figure 17 presents the comparison of the static (E_{stat}) and dynamic elastic Young’s moduli (E_{dyn}). At 600 °C the moduli are almost identical. At 400 °C the Cref-0% moduli is also the same. The remaining points are located above the equivalence curve and are considered to be slightly

overestimated compared with the elastic static modulus. According to Roufael et al.[30], the wave velocity method precisely reflects the evolution of the elastic modulus as a function of temperature.

Figure 18 presents the evolution of the ratio between the moduli of elasticity (E_{stat} and E_{dyn}) and compressive strength (E/f_c) as a function of the temperature. The results showed that the E_{stat}/f_c ratios were between 283 and 568 for Cref-0% concrete, 426 and 593 for RC-5% concrete, 297 and 573 for RC-10% concrete, 277 and 571 for RC-15% concrete, 428 and 587 for RC-20% concrete. The E_{dyn}/f_c ratios are between 240 and 702 for Cref-0% concrete, 236 and 736 for RC-5% concrete, 295 and 706 for RC-10% concrete, 227 and 800 for RC-15% concrete, 472 and 817 for RC-20% concretes. A little decrease in E/f_c ratio is observed between the ambient temperature and 200 °C and then the ratio decreases more significantly from 400 °C up to 600 °C. It is consistent with the appearance of cracks at 600 °C as seen on the tomography images (Fig. 10). It appears that the stiffness of the material is more influenced by the temperature than by the compressive strength, especially

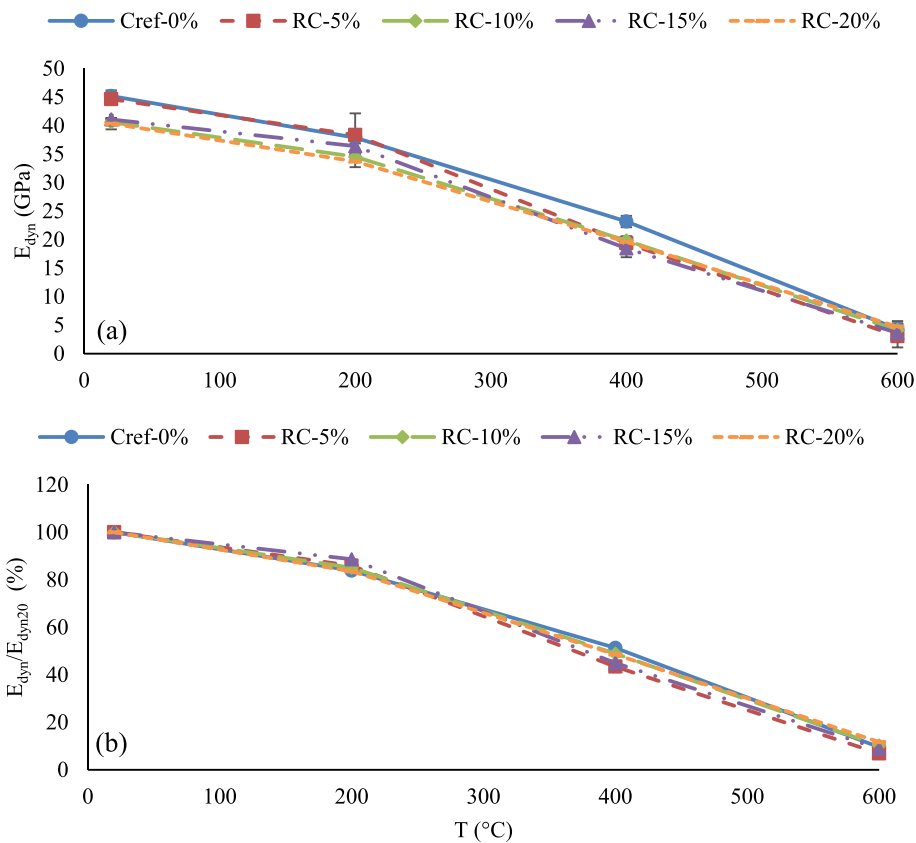


Fig. 16 Absolute (a) and relative (b) residual elastic dynamic modulus of Cref-0%, RC-5%, RC-10%, RC-15%, RC-20% concretes as the function of the temperature

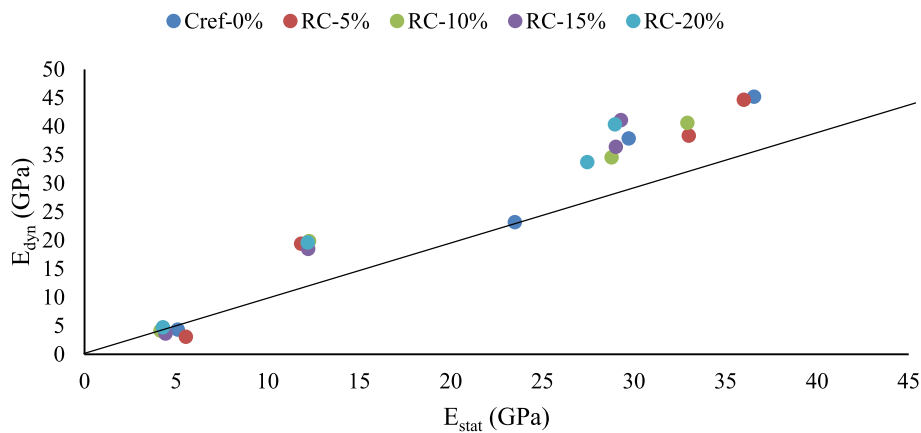


Fig. 17 Dynamic elastic modulus (E_{dyn} [GPa]) vs static elastic modulus (E_{stat} [GPa])

for low cement substitutions. In addition, the elastic modulus decreases gradually with the RF percentage, whereas the compressive strength decreases a little for the 5% and 10% of RF before decreasing further for the highest rates of substitution of cement by recycled fines.

4 Conclusion

The effect of fire on recycled concrete involves irreversible physical and chemical changes which progress with increasing temperature. Cracking sensitivity and pore network evolution can cause the recycled concrete to crack and spall. In this study, the effects of recycled

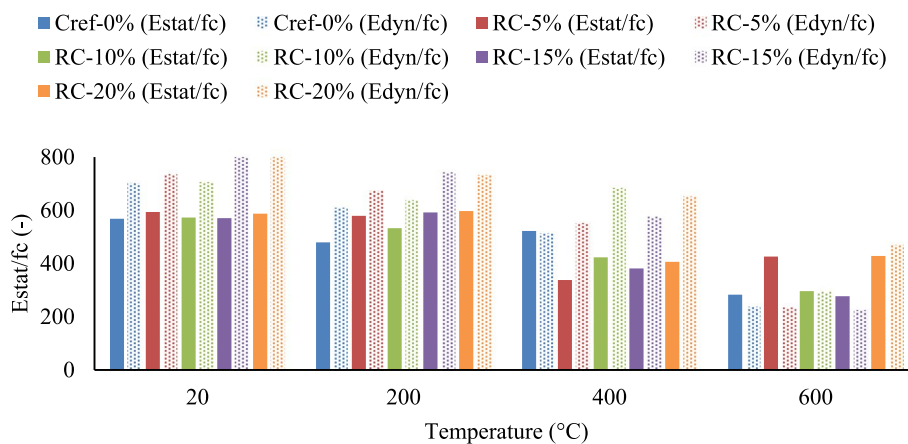


Fig. 18 Relationship between modulus of elasticity and compressive strength

findings on the physical, thermal, and mechanical properties of concrete after heating were investigated. The experimental results revealed the following.

- Physical properties of RC-5% concrete were very close to those of Cref-0% concrete.
- With respect to the thermal properties, the average loss of thermal conductivity during heating was equal for all the concretes. Recycled gravel and/or sand have a greater influence on concrete than recycled fines.
- The increase in conductivity during cooling between 300 °C and 200 °C can be explained by the reversible expansion of aggregates and the compacting of cement paste. The hysteresis that appears during the cooling phase indicates irreversible material degradation.
- The recycled fine concrete showed a higher mass loss and ethanol porosity. This is linked to the higher rate of water loss from the recycled concrete. This is also consistent with the tomography results, which showed a higher cracking rate for recycled concrete. The RC-20% concrete showed the higher porosity evolution from the ambient temperature up to 600 °C.
- The RF replacement ratios reduced the mechanical properties of recycled concrete. At ambient temperatures, the higher the recycled fines, the lower the residual compressive strength and residual elastic modulus of the recycled concrete. When heated beyond 600 °C, the residual mechanical properties of all concretes (including Cref-0% concrete) are low and analogous.

Authors’ contributions

Z. Mesticou and A. Si Larbi contributed to the design of the manuscript. C. Bideux and N. Algourdin carried out data collection and processing. C. Bideux and Z. Mesticou were involved in casting the specimens. N. Algourdin, Z. Mesticou and A. Si Larbi wrote and revised the paper. All authors have read and agreed to the published version of the manuscript.

Funding

This study was funded by Pack Ambition International (PAI) of the Rhône-Alpes and Auvergne Region, FRANCE.

Data Availability

The data that support the findings of this study are available from the corresponding author upon reasonable request.

Declarations

Competing Interests

The authors have no relevant financial or non-financial interests to disclose.

Received: 20 August 2024 Revised: 12 November 2024 Accepted: 13 November 2024
Published online: 03 December 2024

References

1. ADEME (Ecological Transition Agency), & L. Château. (2017). *Construction waste, Technical report*.
2. AFNOR. (2010). Concrete - Testing hardened concrete - Testing porosity and density. *NFP*, 18–459.
3. AFNOR. (2013). Testing hardened concrete. Determination of secant modulus of elasticity in compression. *NF EN, 12390–13*, 18–455.
4. AFNOR. (2012). Tests for hardened concrete - Part 3: Compressive strength of specimens, *NF EN, 12390–3*, 18–455.
5. Alarcon-Ruiz, L., Platret, G., Massieu, E., & Ehlacher, A. (2005). The use of thermal analysis in assessing the effect of temperature on a cement paste. *Cement and Concrete Research*, 35, 609–613.
6. Algourdin, N., Sy Hung, B., Mesticou, Z., & Si Larbi, A. (2020). Effects of high temperature on mechanical behaviour and physicochemical properties of recycled mortars and its components. *Construction and Building Materials*, 248, 118554. <https://doi.org/10.1016/j.conbuildmat.2020.118554>
7. Algourdin, N., Mesticou, Z., & Si Larbi, A. (2021). Characterisation of thermally activated recycled cement and mortars at high temperature.

- International Conference on Mechanical, Materials and Renewable Energy (ICMMRE).*
8. Algourdin, N., Nguyen, Q. N. A., Mesticou, Z., & Si Larbi, A. (2021). Durability of recycled fine mortars under freeze–thaw cycles. *Construction and Building Materials*, 25. <https://doi.org/10.1016/j.conbuildmat.2021.123330>
 9. Algourdin, N., Pliya, P., Beaucour, A. L., Noumowé, A., & di Coste, D. (2022). Effect of fine and coarse recycled aggregates on high-temperature behaviour and residual properties of concrete. *Construction and Building Materials*, 341, 1–14. <https://doi.org/10.1016/j.conbuildmat.2022.127847>
 10. Algourdin, N., Pliya, P., Beaucour, A. L., Simon, A., & Noumowé, A. (2017). Influence of steel and/or polypropylene fibres on the behaviour of concrete at high temperature: Spalling, transfer and mechanical properties. *Construction and Building Materials*, 132, 240–250. <https://doi.org/10.1016/j.conbuildmat.2016.11.120>
 11. Algourdin, N., Sy Hung, B., Mesticou, Z., & Si Larbi, A. (2020). Effects of high temperature on mechanical behaviour and physicochemical properties of recycled mortars and its components. *Construction and Building Materials*, 248, 118554. <https://doi.org/10.1016/j.conbuildmat.2020.118554>
 12. Bogas, J. A., Carriço, A., & Real, S. (2022). Durability of concrete produced with recycled cement from waste concrete. *Materials Today: Proceedings*, 58, 1149–1154. <https://doi.org/10.1016/J.MATPR.2022.01.280>
 13. Brooks, A. L., Zhou, H., & Hanna, D. (2018). Comparative study of the mechanical and thermal properties of lightweight cementitious composites. *Construction and Building Materials*, 159, 316–328. <https://doi.org/10.1016/j.conbuildmat.2017.10.102>
 14. Cardoza, A., & Colorado, H. A. (2023). Alkali-activated cement manufactured by the alkaline activation of demolition and construction waste using brick and concrete wastes. *Open Ceramics*, 16, 100438. <https://doi.org/10.1016/J.OCERAM.2023.100438>
 15. Florea, M. V. A., & Brouwers, H. J. H. (2012). Recycled concrete fines and aggregates- the composition of various size fractions related to crushing history. *Proceedings of the International Conference on Building Materials*, 1034–1041.
 16. Florea, M. V. A., Ning, Z., & Brouwers, H. J. H. (2014). Activation of liberated concrete fines and their application in mortars. *Construction and Building Materials*, 50, 1–12. <https://doi.org/10.1016/j.conbuildmat.2013.09.012>
 17. Francioso, V., Moro, C., & Velay-lizancos, M. (2021). Effect of recycled concrete aggregate (RCA) on mortar's thermal conductivity susceptibility to variations of moisture content and ambient temperature. *Journal of Building Engineering*, 43(August), 103208. <https://doi.org/10.1016/j.jobbe.2021.103208>
 18. Hager, I., & Pimienta, P. (2004). *Mechanical properties of HPC at high temperature. Fib task group 4.3 "Fire design of concrete structures."*
 19. Imbabi, M. S., Carrigan, C., & McKenna, S. (2012). Trends and developments in green cement and concrete technology. *International Journal of Sustainable Built Environment*, 1(2), 194–216. <https://doi.org/10.1016/J.IJSBE.2013.05.001>
 20. Irum, S., & Shabbir, F. (2024). Performance of fly ash/GGBFS based geopolymer concrete with recycled fine and coarse aggregates at hot and ambient curing. *Journal of Building Engineering*, 95. <https://doi.org/10.1016/j.jobbe.2024.110148>
 21. Khaliq, W., & Taimur. (2018). Mechanical and physical response of recycled aggregates high-strength concrete at elevated temperatures. *Fire Safety Journal*, 96, 203–214. <https://doi.org/10.1016/J.FIRESAF.2018.01.009>
 22. Khan, M., Lao, J., Riaz Ahmad, M., Kai, M. F., & Dai, J. G. (2023). The role of calcium aluminate cement in developing an efficient ultra-high performance concrete resistant to explosive spalling under high temperatures. *Construction and Building Materials*, 384, 131469. <https://doi.org/10.1016/J.CONBUILDMAT.2023.131469>
 23. Kim, K. Y., Yun, T. S., & Park, K. P. (2013). Evaluation of pore structures and cracking in cement paste exposed to elevated temperatures by X-ray computed tomography. *Cement and Concrete Research*, 50, 34–40. <https://doi.org/10.1016/j.cemconres.2013.03.020>
 24. Laneyrie, C., Beaucour, A., Green, M. F., Hebert, R. L., Ledesert, B., & Noumowé, A. (2016). *Influence of recycled coarse aggregates on normal and high performance concrete subjected to elevated temperatures.*, 111, 368–378. <https://doi.org/10.1016/j.conbuildmat.2016.02.056>
 25. Liu, Y., Wang, W., Chen, Y. F., & Ji, H. (2016). Residual stress-strain relationship for thermal insulation concrete with recycled aggregate after high temperature exposure. *Construction and Building Materials*, 129, 37–47. <https://doi.org/10.1016/j.conbuildmat.2016.11.006>
 26. AFNOR. (2005). Testing of concrete in structures - Part 4: Determination of sound velocity. *NF EN, 12504–4*.
 27. Nguyen, L. H., Beaucour, A. L., Ortola, S., & Noumowé, A. (2017). Experimental study on the thermal properties of lightweight aggregate concretes at different moisture contents and ambient temperatures. *Construction and Building Materials*, 151, 720–731. <https://doi.org/10.1016/j.conbuildmat.2017.06.087>
 28. Pliya, P., Beaucour, A.-L., & Noumowé, A. (2011). Contribution of cocktail of polypropylene and steel fibres in improving the behaviour of high strength concrete subjected to high temperature. *Construction and Building Materials*, 25(4), 1926–1934. <https://doi.org/10.1016/j.conbuildmat.2010.11.064>
 29. Recommendations, R. I. L. E. M., & 200-HTC. (2007). Recommendation of RILEM TC 200-HTC: Mechanical concrete properties at high temperatures—modelling and applications. *Materials and Structures*, 40(9), 841–853. <https://doi.org/10.1617/s11527-007-9285-2>
 30. Roufael, G., Beaucour, A. L., Eslami, J., Hoxha, D., & Noumowé, A. (2021). Influence of lightweight aggregates on the physical and mechanical residual properties of concrete subjected to high temperatures. *Construction and Building Materials*, 268. <https://doi.org/10.1016/j.conbuildmat.2020.121221>
 31. Salahuddin, H., Nawaz, A., Maqsoom, A., Mehmood, T., Zeeshan, B., & ul A. (2019). Effects of elevated temperature on performance of recycled coarse aggregate concrete. *Construction and Building Materials*, 202, 415–425. <https://doi.org/10.1016/j.conbuildmat.2019.01.011>
 32. Sargam, Y., Wang, K., & Alleman, J. E. (2020). Effects of Modern Concrete Materials on Thermal Conductivity. *Journal of Materials in Civil Engineering*, 32(4). [https://doi.org/10.1061/\(ASCE\)MT.1943-5533.0003026](https://doi.org/10.1061/(ASCE)MT.1943-5533.0003026)
 33. Shui, Z., Xuan, D., Chen, W., Yu, R., & Zhang, R. (2009). Cementitious characteristics of hydrated cement paste subjected to various dehydration temperatures. *Construction and Building Materials*, 23(1), 531–537. <https://doi.org/10.1016/j.conbuildmat.2007.10.016>
 34. Shui, Z., Xuan, D., Wan, H., & Cao, B. (2008). Rehydration reactivity of recycled mortar from concrete waste experienced to thermal treatment. *Construction and Building Materials*, 22, 1723–1729. <https://doi.org/10.1016/j.conbuildmat.2007.05.012>
 35. Silva, R. V., De Brito, J., & Dhir, R. K. (2016). Establishing a relationship between modulus of elasticity and compressive strength of recycled aggregate concrete. *Journal of Cleaner Production*, 112, 2171–2186. <https://doi.org/10.1016/j.jclepro.2015.10.064>
 36. Xi, X., Zheng, Y., Zhuo, J., Zhang, P., Golewski, G. L., & Du, C. (2024). Mechanical properties and hydration mechanism of nano-silica modified alkali-activated thermally activated recycled cement. *Journal of Building Engineering*, 98. <https://doi.org/10.1016/j.jobbe.2024.110998>
 37. Xuan, D., Zhan, B., & Poon, C. S. (2018). Thermal and residual mechanical profile of recycled aggregate concrete prepared with carbonated concrete aggregates after exposure to elevated temperatures. *Fire and Materials*, 42(1), 134–142. <https://doi.org/10.1002/fam.2465>
 38. Zanolletto, M., Balducci, R., John, V. M., & Angulo, S. C. (2023). Strength-porosity correlation and environmental analysis of recycled Portland cement. *Resources, Conservation and Recycling*, 190. <https://doi.org/10.1016/j.resconrec.2022.106763>

Publisher's Note

Springer Nature remains neutral with regard to jurisdictional claims in published maps and institutional affiliations.